The 18-kDa Mitochondrial Translocator Protein in Human Gliomas: An ^{11}C-(*R*)PK11195 PET Imaging and Neuropathology Study

Zhangjie Su*[1], Federico Roncaroli*[2], Pascal F. Durrenberger[2], David J. Coope[1,3], Konstantina Karabatsou[3], Rainer Hinz[1], Gerard Thompson[1], Federico E. Turkheimer[4], Karolina Janczar[2], Daniel Du Plessis[5], Andrew Brodbelt[6], Alan Jackson[1], Alexander Gerhard[1], and Karl Herholz[1]

[1]*Wolfson Molecular Imaging Center, University of Manchester, Manchester, United Kingdom;* [2]*Division of Brain Science, Imperial College London, London, United Kingdom;* [3]*Department of Neurosurgery, Salford Royal NHS Foundation Trust, Salford, United Kingdom;* [4]*Center for Neuroimaging, Institute of Psychiatry, King's College London, London, United Kingdom;* [5]*Neuropathology Unit, Salford Royal NHS Foundation Trust, Salford, United Kingdom; and* [6]*Department of Neurosurgery, The Walton Center NHS Foundation Trust, Liverpool, United Kingdom*

The 18-kDa mitochondrial translocator protein (TSPO) is upregulated in high-grade astrocytomas and can be imaged by PET using the selective radiotracer ^{11}C-(*R*)PK11195. We investigated ^{11}C-(*R*)PK11195 binding in human gliomas and its relationship with TSPO expression in tumor tissue and glioma-associated microglia/macrophages (GAMs) within the tumors. **Methods:** Twenty-two glioma patients underwent dynamic ^{11}C-(*R*)PK11195 PET scans and perfusion MR imaging acquisition. Parametric maps of ^{11}C-(*R*)PK11195 binding potential (BP_{ND}) were generated. Co-registered MR/PET images were used to guide tumor biopsy. The tumor tissue was quantitatively assessed for TSPO expression and infiltration of GAMs using immunohistochemistry and double immunofluorescence. The imaging and histopathologic parameters were compared among different histotypes and grades and correlated with each other. **Results:** BP_{ND} of ^{11}C-(*R*)PK11195 in high-grade gliomas was significantly higher than in low-grade astrocytomas and low-grade oligodendrogliomas. TSPO in gliomas was expressed predominantly by neoplastic cells, and its expression correlated positively with BP_{ND} in the tumors. GAMs only partially contributed to the overall TSPO expression within the tumors, and TSPO expression in GAMs did not correlate with tumor BP_{ND}. **Conclusion:** PET with ^{11}C-(*R*)PK11195 in human gliomas predominantly reflects TSPO expression in tumor cells. It therefore has the potential to effectively stratify patients who are suitable for TSPO-targeted treatment.

Key Words: translocator protein; ^{11}C-(*R*)PK11195; glioma; microglia; PET

J Nucl Med 2015; 56:512–517
DOI: 10.2967/jnumed.114.151621

Low- and high-grade gliomas (LGG and HGG, respectively) are the most common primary brain tumors in adults. Their outcome depends on patients' age, tumor location, histotype, and grade. Therapeutic options include surgery, radiotherapy, and chemotherapy but their intra- and intertumoral genetic, epigenetic, molecular, and metabolic heterogeneity represents a challenge for their treatment planning (*1*). An individualized approach has therefore been advocated to more effectively target cancer cells, but such an approach requires adequate stratification of patients. The term theranostics has recently been introduced as a conceptual framework to develop diagnostic tests that directly lead to the application of targeted therapies (*2,3*). In this respect, molecular imaging can be instrumental to personalized treatment to assess the biodistribution and pharmacokinetics of drugs and to determine their efficacy and safety in the treatment of cancer patients (*4*).

The 18-kDa mitochondrial translocator protein (TSPO) is a promising candidate for a theranostic approach of gliomas as it can be visualized and quantified with PET and because it is highly expressed in astrocytomas (*5,6*), but its expression is low in the normal brain. In view of this evidence, experimental studies proposed the TSPO as a target for selective delivery of anticancer drugs into glioma cells or to be exploited as a transporter of drug-containing nanoparticles (*7–9*). TSPO upregulation in cancer cells and its function in their growth, survival, and migration have recently attracted considerable attention (*10*).

By combining PET imaging and analysis of tumor tissue, we aimed to characterize the cell source of TSPO in LGGs and HGGs, and understand the potential of such TSPO imaging in detecting anaplastic transformation of LGGs and stratifying patients who could be eligible for TSPO-targeted treatment. The evidence that the single nucleotide polymorphism in exon 4 of the TSPO gene affects the binding of second-generation ligands (*11*) led us to opt for ^{11}C-(*R*)PK11195 (1-(2-chlorophenyl)-*N*-methyl-*N*-(1-methylpropyl)-3-isoquinoline carboxamide). In addition, most second-generation TSPO ligands have been used only in experimental animals and are not fully characterized in humans (*12–14*). In our previous study, we have demonstrated that ^{11}C-(*R*)PK11195 is a suitable radiotracer for glioma imaging (*15*). In the present study, we hypothesized that TSPO expression in gliomas differs between tumor

Received Nov. 14, 2014; revision accepted Feb. 6, 2015.
For correspondence or reprints contact: Karl Herholz, Wolfson Molecular Imaging Center, University of Manchester, 27 Palatine Rd., Manchester, United Kingdom M20 3LJ.
E-mail: karl.herholz@manchester.ac.uk
*Contributed equally to this work.
Published online Feb. 26, 2015.

grades and histotypes, which could be detected by ^{11}C-(*R*)PK11195 PET imaging; this neuroimaging modality has the potential to identify transforming LGGs and be used to stratify patients for TSPO-targeted treatment that would challenge neoplastic cells.

MATERIALS AND METHODS

Patient Selection

We recruited patients with intraaxial supratentorial, hemispheric tumors consistent with World Health Organization (WHO) grade II and III glioma on structural and perfusion MR imaging scans with the aim to investigate the change associated with anaplastic transformation. As a comparison, we also investigated 2 lesions with obvious neuroimaging features of glioblastoma multiforme (GBM). Overall, 24 patients were enrolled in this study. One patient was excluded because no surgical procedure was performed soon after the PET scan and another excluded because histologic diagnosis was ganglioglioma, leaving 22 patients (mean age, 39 y; range, 22–62 y; 6 women) for analysis. None of the patients had concurrent disease; was on benzodiazepine medication; or had surgical intervention, radiotherapy, or chemotherapy before PET scanning. Nine patients received dexamethasone, but the medication was withdrawn 2 wk before PET scanning, except in 2 patients for whom the discontinuation was felt contraindicated. Detailed demographic and clinical findings are reported in Supplemental Table 1 (supplemental materials are available at http://jnm.snmjournals.org).

This study was approved by the Wrightington, Wigan and Leigh Ethics Committee, and all subjects signed a written informed consent form. Permission to administer radioisotopes was granted by the Administration of Radioactive Substances Advisory Committee of the Department of Health (ARSAC), U.K.

Neuroimaging Studies

MR Imaging. Volumetric MR imaging was performed within 1 mo before PET scanning (median, 5 d; range, 0–31 d) using a 3.0-T scanner (Philips Achieva; Philips Medical System). Standard anatomic sequences were acquired: 3-dimensional T1-weighted gradient-echo sequence (repetition time [TR]/echo time [TE], 500/10 ms; matrix, 512 × 512; slice thickness, 4 mm), 2-dimensional T2-weighted turbo spin-echo sequence (TR/TE, 3,000/80 ms; matrix, 1,024 × 1,024; slice thickness, 3 mm), T2-weighted fluid-attenuated inversion recovery sequence (TR/TE/inversion time, 11,000/120/2,800 ms; matrix, 512 × 512; slice thickness, 3 mm), and postcontrast T1-weighted images (TR/TE, 9.85/4.6 ms; matrix, 224 × 224; slice thickness, 1 mm; flip angle, 8°) after intravenous gadolinium (Dotarem; Guerbet Laboratories) administration (0.1 mmol/kg at 4 mL/s). Additionally, T2*-weighted dynamic susceptibility contrast-enhanced MR imaging (TR/TE, 16.8/24.8 ms; matrix, 80 × 80; slice thickness, 3 mm; flip angle, 7°; temporal resolution, 1.71 s; number of dynamic acquisitions, 60) was performed in 20 patients.

PET. ^{11}C-(*R*)PK11195 was synthesized according to established methods (*16,17*). PET scans were obtained on the High Resolution Research Tomograph (Siemens/CTI) as described previously (*15*). The injected dose of ^{11}C-(*R*)PK11195 was 509 ± 123 MBq, with a specific radioactivity of 132 ± 49GBq/μmol. Data acquisition and reconstruction were also conducted as described previously (*15*). The voxel size of reconstructed PET images was 1.22 × 1.22 × 1.22 mm. Postreconstruction images were regularized with a 3-dimensional gaussian filter of 4 mm in full width at half maximum to reduce image noise on the voxel level.

Image Analysis. Each individual MR image was coregistered with the summed PET image (*18*). The quality of coregistration was visually inspected for accurate anatomic colocalization. Parametric maps of ^{11}C-(*R*)PK11195 binding potential (BP_{ND}, representing the ratio of the specifically bound radioligand over the nondisplaceable one in tissue at equilibrium (*19*)) were calculated using the simplified reference tissue model (*20*), with the cerebellar gray matter providing the reference tissue input function (*15*).

Tumors and the surrounding visible edema were manually delineated on the coregistered T2-weighted fluid-attenuated inversion recovery MR image and confirmed against the T1-weighted postcontrast MR image. The tumor region of interest was projected onto the BP_{ND} parametric map for sampling the mean BP_{ND} value of the entire tumor.

T2* dynamic susceptibility contrast-enhanced MR imaging data were analyzed according to established methods (*21,22*). Cerebral blood flow (CBV) maps were calculated by numeric integration of the area under the concentration time curve from the arrival to recirculation of the contrast bolus (*23*). The CBV map was coregistered to the T1-weighted postcontrast MR image that had already been registered to the summed PET image. Tumor blood volume was quantified using rCBV (CBV relative to the normal-appearing white matter in the contralateral cerebral hemisphere). The whole-tumor region of interest was further edited to exclude areas of large vessels, when present, and projected onto the rCBV map to sample the mean rCBV value of the entire tumor.

Coregistered MR/PET images were used to guide tumor biopsy from areas of contrast enhancement (CE) and high as well as low BP_{ND} or rCBV.

Neuropathology Assessment

The sample comprised 13 astrocytomas (6 grade II, 4 grade III, 3 grade IV) and 9 oligodendrogliomas (7 grade II, 2 grade III). Tumors were graded according to the current WHO criteria (*24*). All oligodendrogliomas and 6 astrocytomas were positive for $IDH1^{R132H}$. The Ki-67 index ranged from 1% to 30% (mean, 7%) and increased with the tumor grade ($P = 0.023$). All oligodendrogliomas showed loss of heterozygosity 1p19q; 1 GBM had 19q deletion with intact 1p. Detained clinicopathologic features are reported in Supplemental Table 1.

The expression of TSPO in neoplastic and nonneoplastic cells and the extent of glioma-associated microglia and macrophages (GAMs), astrocytosis, and microvascular proliferation were evaluated using immunohistochemistry and double immunofluorescence (DIF) in 21 cases (the sample from a WHO II oligodendroglioma was too small) with antibodies directed against the calcium-binding adapter molecule 1 (Iba1) for GAMs, glial acid fibrillary protein and excitatory amino-acid transporter 2 for astrocytes, and CD31 for endothelium. DIF was used to distinguish TSPO-positive in neoplastic and nonneoplastic cells. To compare PET imaging results and TSPO expression in tissue, we quantified the density of TSPO-positive cells and Iba1-positive GAMs of each tumor and represented the value as percentage of positive cells against overall cell density × 0.25 mm^2. The density of TSPO-positive GAMs × 0.25 mm^2 was calculated with DIF. As a surrogate marker of TSPO content in tissue, we also measured the intensity and surface of cytoplasmic TSPO immunolabeling after a threshold of intensity based on endothelial expression was selected. For all measurements, counting was duplicated by a second observer and correlated for interobserver variability. Detailed protocols for neuropathology assessment are reported in the Supplemental Methods section.

Statistical Analysis

For statistical analysis, tumors were grouped as low-grade astrocytomas (LGAs, $n = 6$), low-grade oligodendrogliomas (LGOs, $n = 7$), and HGGs (including 7 high-grade astrocytomas and 2 anaplastic oligodendrogliomas [AOs]). Imaging and pathology parameters were compared by the Kruskal–Wallis test and by Pearson correlation analysis using SPSS 13.0 (IBM).

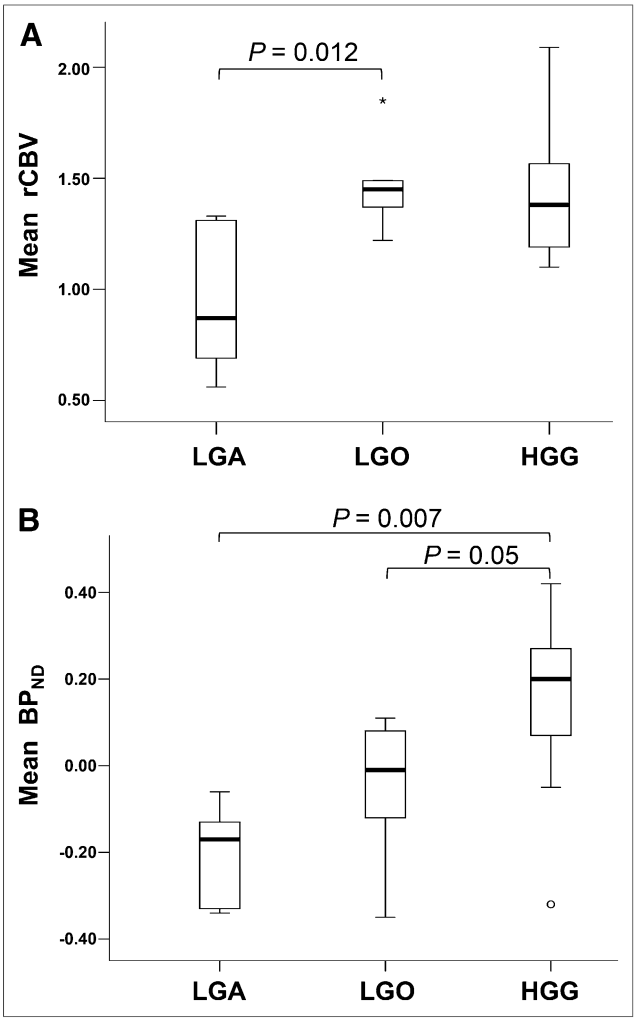

FIGURE 1. Box plot of mean rCBV (A) and ^{11}C-(*R*)PK11195 BP_{ND} (B) in different grades and types of gliomas.

RESULTS

MR Imaging: CE and rCBV

Substantial intratumoral CE was observed in 2 GBMs, whereas CE was absent or minor in most tumors (Supplemental Table 1). rCBV maps showed considerable heterogeneity within tumors, and small foci of increased rCBV within the tumor were observed in 5 LGOs and 1 LGA. A significant grouping effect was found in mean rCBV ($P = 0.032$), wherein LGOs showed a higher mean rCBV than that of LGAs ($P = 0.012$) and did not differ from HGGs ($P = 0.406$, Fig. 1A).

PET Scanning with ^{11}C-(*R*)PK11195

As a whole, LGGs (LGAs plus LGOs) demonstrated a mean BP_{ND} of ^{11}C-(*R*)PK11195 significantly lower than HGGs ($P = 0.006$). ^{11}C-(*R*)PK11195 binding within LGGs appeared even lower than that in the surrounding cerebral cortex (Fig. 2A). A significant grouping effect was also found in mean BP_{ND} among the 3 groups ($P = 0.008$). Post hoc analysis revealed lower mean BP_{ND} values in LGAs and LGOs than HGGs ($P = 0.007$ and 0.05, respectively, Fig. 1B), and the difference in mean BP_{ND} between LGAs and LGOs was not significant ($P = 0.063$) though the values tended to be higher in the latter. BP_{ND} values of LGOs were lower than the 2 AOs. Small foci of high BP_{ND} were present in 7 LGGs, 5 of which were oligodendrogliomas (Fig. 2A). There were no significant differences in the cold (*R*)-PK11195 injected among all groups.

Four tumors displayed faint or no CE but pronounced ^{11}C-(*R*) PK11195 binding (Fig. 2B). These 4 cases were all confirmed to be HGGs postoperatively. In all the tumors with CE, areas of increased BP_{ND} always exceeded areas of CE. Small foci of increased rCBV seen in LGGs did not colocalize with small foci of increased BP_{ND}, whereas 5 HGGs demonstrated high rCBV foci colocalized with focal CE and high BP_{ND}. Overall, mean BP_{ND} and mean rCBV were moderately correlated ($r^2 = 0.38$, $P = 0.005$).

Neuropathologic Assessment

TSPO-positive cells showed cytoplasmic, granular TSPO immunolabeling consistent with mitochondrial location. No convincing nuclear expression was observed. TSPO-positive cells were evenly distributed in the tumor mass as well as in its peripheral, infiltrative component, and their average density ranged between 9 and 87 cells × 0.25 mm^2, accounting for 1.7%–38.6% of the overall cell population. DIF experiments demonstrated that TSPO was predominantly expressed in neoplastic cells (Supplemental Fig. 1; Supplemental Table 2). The number of TSPO-positive neoplastic cells increased with the WHO grade, but the trend did not reach statistical significance ($P = 0.064$). The surface of TSPO-positive cytoplasms measured by intensity of expression varied between cases ranging between 0.77% and 6.07% (mean, 2.18%; median, 1.50%). When grouped by WHO grade and histotype, the average value significantly increased with grade ($P = 0.007$) (Fig. 3; Supplemental Table 2), being higher in HGGs than LGAs and LGOs ($P = 0.025$ and 0.007, respectively), although the expression in 2 anaplastic astrocytomas (AAs) overlapped LGAs with values of 1.95%

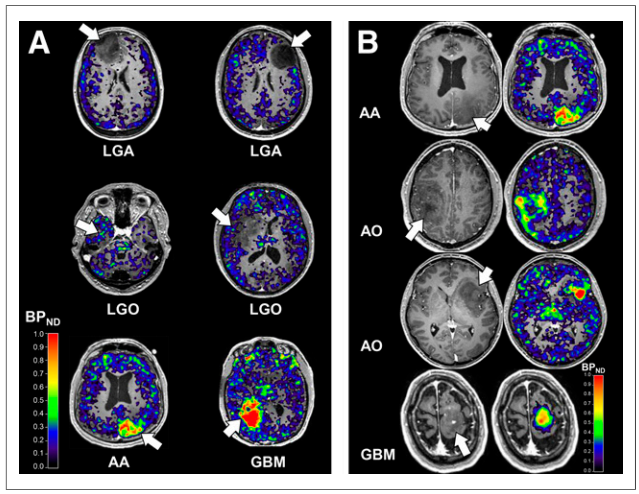

FIGURE 2. (A) Coregistered and fused postcontrast T1-weighted MR images (gray scale) and parametric BP_{ND} images (spectrum color scale) of representative cases of LGA, LGO, and HGG; BP_{ND} is low in LGAs whereas high BP_{ND} foci are found in LGOs and high BP_{ND} areas in HGGs (arrows). (B) Coregistered postcontrast T1-weighted MR images and parametric BP_{ND} images in 4 HGGs showing little or no contrast enhancement (arrows) and high ^{11}C-(*R*)PK11195 binding within tumors. Color bars denote BP_{ND} values.

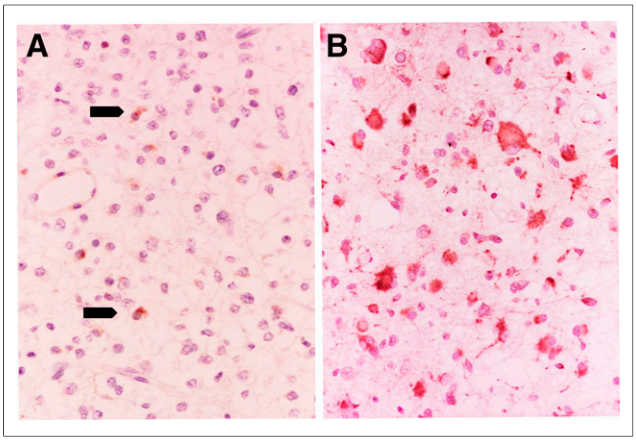

FIGURE 3. Tissue analysis of TSPO expression in different tumor histotypes and grades using immunohistochemistry. Examples shown are LGO (A) and AA (B) in TSPO immunoperoxidase immunohistochemistry, ×20. Neoplastic cells in LGO show rim of positive cytoplasm (arrows) whereas neoplastic cells in the case of AA show large, intensely positive cytoplasm reflecting higher TSPO content.

and 1.03%, respectively. TSPO expression did not differ between LGAs and LGOs.

GAMs accounted for 7.5%–44.4% of the overall cell density and their density also showed a trend to increase with the WHO grade ($P = 0.054$) (Fig. 4), but DIF demonstrated that only a proportion of GAMs ranging between 4.2% and 55.8% expressed TSPO (mean, 16.9%) (Figs. 4C and 4D; Supplemental Fig. 1; Supplemental Table 2) and that TSPO-positive GAMs accounted for part of the overall TSPO cell population (mean, 21.7%; range, 4.2%–55%). Neither the density of total GAMs nor the density of TSPO-positive GAMs differed among the 3 groups (LGAs, LGOs, and HGGs).

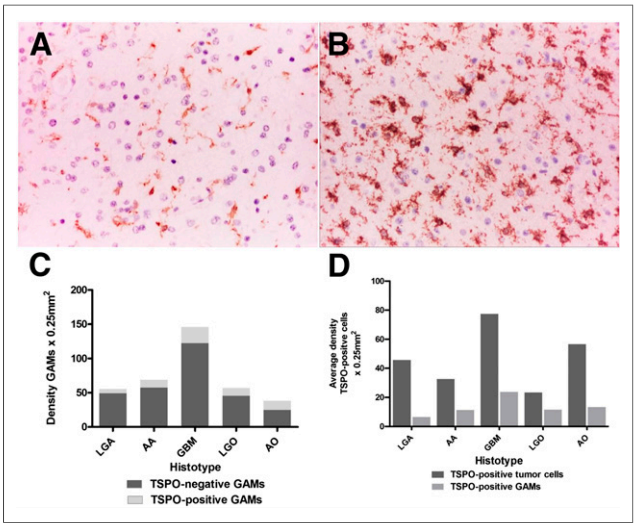

FIGURE 4. Overall distribution of GAMs and TSPO-positive GAMs in different tumor histotypes and grades. Examples shown are LGA (A) and AA (B) in Iba1 immunoperoxidase immunohistochemistry, ×20, where less Iba1-positive stain is observed in LGA than AA, indicating increase of GAMs with tumor grade. (C) Density (per 0.25 mm^2) of TSPO-positive and TSPO-negative GAMs in different tumor histotypes and grades. (D) Average density of TSPO-positive neoplastic cells and TSPO-positive GAMs in different tumor histotypes and grades.

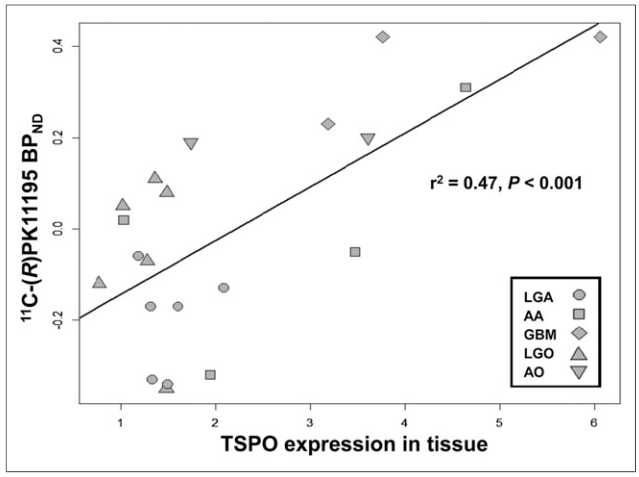

FIGURE 5. Bivariate correlation between TSPO expression in glioma tissue and mean BP_{ND} of ^{11}C-(*R*)PK11195 in tumors.

No TSPO expression was identified in reactive astrocytes (Supplemental Fig. 2). Endothelial and smooth muscle cells of normal vessels entrapped in neoplastic tissue were TSPO-positive irrespective of tumor histotype and grade. In contrast, TSPO expression was low to absent in newly formed vessels seen in the cases of GBM (Supplemental Fig. 2).

Tumor BP_{ND} correlated with the surface of TSPO-positive cytoplasms ($r^2 = 0.47$, $P < 0.001$, Fig. 5) and the density of TSPO-positive neoplastic cells ($r^2 = 0.30$, $P = 0.01$) but not with TSPO-positive GAMs. These positive correlations became stronger in HGGs ($r^2 = 0.57$ and $r^2 = 0.55$) but were not significant in LGAs or LGOs, when different tumor types and grades were investigated independently. Our results altogether confirm that ^{11}C-(*R*)PK11195 binds predominantly TSPO in neoplastic cells, with only a minor interference from microenvironment.

DISCUSSION

In this study, we have investigated the suitability of PET imaging to stratify gliomas with low and high TSPO expression and its potential to identify anaplastic transformation of LGGs. PET imaging findings were compared with structural and perfusion MR imaging and were validated with tissue analysis. Our results demonstrated an excellent correlation between TSPO in tumor cells and ^{11}C-(*R*)PK11195 binding, indicating the potential of TSPO imaging for patient stratification and detection of tumor progression.

The binding of ^{11}C-(*R*)PK11195 and tissue expression of TSPO were low in LGGs. Similar to our result, a previous autoradiography study (*25*) documented lower intratumoral binding in LGGs than GBM but, unlike our imaging study, did not examine PK11195 binding in normal tissue of the same patients with LGA. We even observed negative numeric values in LGGs, suggesting that the cerebellum as the reference region had higher residual TSPO binding than the LGGs. Although this is a limitation for our ability to measure the absolute level of binding potentials, it does not appear to be critical for relative comparison between different tumors and for identification of patients with high TSPO expression in tumor cells, who could potentially benefit from TSPO-targeted treatment. The results did not depend on the choice of the reference region. Even when using the supervised cluster

technique, though not preferred for gliomas for reasons reported in the previous methodologic study (*15*), we obtained essentially the same results.

In the interpretation of results we also considered potential confounding factors. Most malignant gliomas show disruption of the blood–brain barrier (BBB), which could affect tracer uptake. Because of our selection criteria, we included several HGGs with little or no BBB disruption (as demonstrated by absence or mild focally restricted CE on MR imaging) as well as 2 GBMs with extensive CE. The spatial extent of increased tracer binding always exceeded the extent of CE, and 4 of the 5 nonenhancing HGGs demonstrated high ^{11}C-(*R*)PK11195 binding, indicating the independence of increased binding from BBB disruption and the possibility of TSPO imaging in early detection of malignant transformation. In our previous methodologic study, we already demonstrated by kinetic analysis of ^{11}C-(*R*)PK11195 uptake in these tumors that tracer extraction from blood to tumor tissue does not depend on tumor grade or BBB breakdown (*15*), probably because of tracer lipophilicity.

When histotypes were examined separately, LGOs showed higher ^{11}C-(*R*)PK11195 binding than expected from tissue analysis. The reason for this discrepancy is not clear, but it is likely due to the higher vascular density of LGO (*21*), which was also evident in our rCBV measurements. Although endothelial TSPO expression was similar to LGAs, the increased number of vessels could explain the apparent high BP_{ND} in LGOs because vessels were not included in TSPO quantification on tissue. Higher tracer uptake in oligodendrogliomas than in astrocytomas of the same grade has been noted for other tracers, including ^{18}F-FDG and amino acids (*26,27*). The calculation of the BP_{ND} using the simplified reference tissue model includes a correction for possible differences in transport, which could be caused by the differences in vasculature. When we included a correction for local blood volume as suggested by Tomasi et al. (*28*), the results were similar whereas the variation of estimated parameters increased.

Though limited to a few cases, our results showed increased ^{11}C-(*R*)PK11195 PET and tissue expression in anaplastic gliomas, suggesting that TSPO imaging can be used to detect anaplastic transformation in LGGs, which is especially interesting and promising in oligodendroglial tumors. In our study, rCBV analysis did not reveal significant differences between LGOs and AOs or other high-grade astrocytomas. Preoperative distinction between LGOs and AOs is challenging with structural and physiologic imaging, and correct grading can also be difficult at histology. A few PET imaging studies have investigated oligodendroglial tumors, and to our knowledge none has used ^{11}C-(*R*)PK11195. ^{18}F-FDG and ^{11}C-methionine or both ligands in combination demonstrated generally high tracer uptake of oligodendrogliomas irrespective of their WHO grade (*29,30*).

We demonstrated a quantitative correlation between in vivo PET imaging and TSPO in tissue evaluated by immunohistochemistry and DIF, and as expected we observed an overall significant correlation between tumor grade and TSPO binding although not all AAs show high tracer uptake. One AA in particular showed negative BP_{ND}. This tumor was a transforming astrocytoma in which anaplastic features were limited to a small component of the lesion, and the overall TSPO expression was as low as LGAs. Our results on tissue are consistent with previous studies that used immunohistochemistry to investigate TSPO in human astrocytomas (*31,32*) and documented variability in TSPO expression and some degree of overlap between WHO grade II and III lesions.

Tissue analysis in this study was based on paraffin-embedded tissue. For this reason, we could not perform affinity analysis and quantification of TSPO protein content. To overcome this limitation we used 3 different approaches and correlated them to PET imaging. We first measured the number of TSPO-positive cells against the total cell population and then estimated the number of TSPO-positive cells per surface unit. These 2 approaches showed a trend toward or reaching significance but did not take into account the density of TSPO in cell cytoplasm. As a surrogate measure of TSPO density, we therefore opted to measure the intensity and surface of TSPO-positive cytoplasm per surface unit. This method proved to correlate significantly with imaging data as it more accurately reflected the amount of TSPO and therefore the binding sites available in the cell cytoplasm. Notably, values below 1.5% in tissue correlated with absence of detectable ^{11}C-(*R*)PK11195 uptake.

To our knowledge, this study is the first to comprehensively address the question of TSPO expression in both neoplastic and nonneoplastic cells in human gliomas and quantify expression in the different cell populations. Similar to previous studies (*14,33*), we demonstrated that TSPO is predominantly expressed in neoplastic cells, with GAMs only partially contributing to PET signal and no expression in reactive astrocytes. We also demonstrated that TSPO was detectable only in a subpopulation of microglia and macrophages, overall accounting for about 16% of GAMs. This observation overcomes the general assumption from studies on neurodegenerative and neuroinflammatory conditions that almost all activated microglial cells are TSPO-positive and therefore that a high proportion of ^{11}C-(*R*)PK11195 binding relates to microglial TSPO (*34,35*). The reason for TSPO downregulation in GAMs is unclear. Although animal models documented reduced microglial TSPO (*36*) and reduced ^{3}H-PK11195 binding (*37*) after steroid administration, TSPO downregulation in GAMs did not depend on preoperative dexamethasone because only 2 patients were on the medication throughout the study and their BP_{ND} as well as TSPO-positive GAMs were not low, compared with other cases.

CONCLUSION

PET with ^{11}C-(*R*)PK11195 in human gliomas predominantly reflects TSPO expression in tumor cells. We proved that TSPO imaging has the potential to detect early anaplastic transformation of LGGs, and it can be effective to stratify patients with glioma who are suitable for TSPO-targeted treatment. The evidence that not all AAs show high TSPO further supports the role of TSPO imaging for patient selection. The need for overcoming the BBB to deliver drugs within the central nervous system has further increased the focus on TSPO, as its ligands are highly lipophilic and therefore easily cross an intact BBB. The identification of biomarkers that allow patient stratification and monitoring of disease progression and response to treatment is one of the major challenges of molecular imaging and the central paradigm of theranostics.

DISCLOSURE

The costs of publication of this article were defrayed in part by the payment of page charges. Therefore, and solely to indicate this fact, this article is hereby marked "advertisement" in accordance with 18 USC section 1734. The research leading to these

results received funding from the European Union's Seventh Framework Program (FP7/2007-2013) under grant agreement HEALTH-F2-2011-278850 (INMiND), the Manchester Integrating Medicine and Innovative Technology program (Science Bridges Project R108094), and the Astro Fund. This work was also partly supported by the Brain Tumor Research Campaign (BTRC) charity. Control cases of multiple sclerosis were provided by the U.K. Multiple Sclerosis Society Tissue Bank at Imperial College London, funded by the U.K. Multiple Sclerosis Society. No other potential conflict of interest relevant to this article was reported.

ACKNOWLEDGMENTS

We thank the patients who participated in this study and the staff involved in the scanning, especially Dr. Adam McMahon and Michael Green for radioligand synthesis, Jose Anton for image reconstruction, and the radiographers Eleanor Duncan-Rouse and Gerrit Helms Van Der Vegte. Ajit Sofat, James Leggate, Dr. Ioannis Trigonis, Dr. Calvin Soh, Michael Jenkinson, Dr. Kumar Das, and Dr. Daniel Crooks provided clinical support and/or helped with patient identification/recruitment.

REFERENCES

1. Weller M, Pfister SM, Wick W, Hegi ME, Reifenberger G, Stupp R. Molecular neuro-oncology in clinical practice: a new horizon. *Lancet Oncol.* 2013;14:e370–e379.
2. Olar A, Aldape KD. Using the molecular classification of glioblastoma to inform personalized treatment. *J Pathol.* 2014;232:165–177.
3. Terreno E, Uggeri F, Aime S. Image guided therapy: the advent of theranostic agents. *J Control Release.* 2012;161:328–337.
4. Ding H, Wu F. Image guided biodistribution and pharmacokinetic studies of theranostics. *Theranostics.* 2012;2:1040–1053.
5. Scarf AM, Kassiou M. The translocator protein. *J Nucl Med.* 2011;52:677–680.
6. Han Z, Slack RS, Li W, Papadopoulos V. Expression of peripheral benzodiazepine receptor (PBR) in human tumors: relationship to breast, colorectal, and prostate tumor progression. *J Recept Signal Transduct Res.* 2003;23:225–238.
7. Austin CJ, Kahlert J, Kassiou M, Rendina LM. The translocator protein (TSPO): a novel target for cancer chemotherapy. *Int J Biochem Cell Biol.* 2013;45:1212–1216.
8. Denora N, Laquintana V, Trapani A, et al. Translocator protein (TSPO) ligand-Ara-C (cytarabine) conjugates as a strategy to deliver antineoplastic drugs and to enhance drug clinical potential. *Mol Pharm.* 2010;7:2255–2269.
9. Musacchio T, Laquintana V, Latrofa A, Trapani G, Torchilin VP. PEG-PE micelles loaded with paclitaxel and surface-modified by a PBR-ligand: synergistic anticancer effect. *Mol Pharm.* 2009;6:468–479.
10. Owen DR, Yeo AJ, Gunn RN, et al. An 18-kDa Translocator protein (TSPO) polymorphism explains differences in binding affinity of the PET radioligand PBR28. *J Cereb Blood Flow Metab.* 2012;32:1–5.
11. Buck JR, McKinley ET, Hight MR, et al. Quantitative, preclinical PET of translocator protein expression in glioma using ^{18}F-*N*-fluoroacetyl-*N*-(2,5-dimethoxybenzyl)-2-phenoxyaniline. *J Nucl Med.* 2011;52:107–114.
12. Tang D, Hight MR, McKinley ET, et al. Quantitative preclinical imaging of TSPO expression in glioma using *N,N*-diethyl-2-(2-(4-(2-^{18}F-fluoroethoxy)phenyl)-5,7-fimethylpyrazolo[1,5-a]pyrimidin-3-yl)acetamide. *J Nucl Med.* 2012;53:287–294.
13. Winkeler A, Boisgard R, Awde AR, et al. The translocator protein ligand [^{18}F] DPA-714 images glioma and activated microglia in vivo. *Eur J Nucl Med Mol Imaging.* 2012;39:811–823.
14. Su Z, Herholz K, Gerhard A, et al. [^{11}C]-(*R*)PK11195 tracer kinetics in the brain of glioma patients and a comparison of two referencing approaches. *Eur J Nucl Med Mol Imaging.* 2013;40:1406–1419.
15. Cremer JE, Hume SP, Cullen BM, et al. The distribution of radioactivity in brains of rats given [N-methyl-^{11}C]PK 11195 in vivo after induction of a cortical ischaemic lesion. *Int J Rad Appl Instrum B.* 1992;19:159–166.
16. Shah F, Hume SP, Pike VW, Ashworth S, McDermott J. Synthesis of the enantiomers of [N-methyl-^{11}C]PK 11195 and comparison of their behaviours as radioligands for PK binding sites in rats. *Nucl Med Biol.* 1994;21:573–581.
17. Cízek J, Herholz K, Vollmar S, Schrader R, Klein J, Heiss WD. Fast and robust registration of PET and MR images of human brain. *Neuroimage.* 2004;22:434–442.
18. Innis RB, Cunningham VJ, Delforge J, et al. Consensus nomenclature for in vivo imaging of reversibly binding radioligands. *J Cereb Blood Flow Metab.* 2007;27:1533–1539.
19. Lammertsma AA, Hume SP. Simplified reference tissue model for PET receptor studies. *Neuroimage.* 1996;4:153–158.
20. Cha S, Tihan T, Crawford F, et al. Differentiation of low-grade oligodendrogliomas from low-grade astrocytomas by using quantitative blood-volume measurements derived from dynamic susceptibility contrast-enhanced MR imaging. *AJNR.* 2005;26:266–273.
21. Wetzel SG, Cha S, Johnson G, et al. Relative cerebral blood volume measurements in intracranial mass lesions: interobserver and intraobserver reproducibility study. *Radiology.* 2002;224:797–803.
22. Spampinato MV, Smith JK, Kwock L, et al. Cerebral blood volume measurements and proton MR spectroscopy in grading of oligodendroglial tumors. *AJR.* 2007;188:204–212.
23. Louis DN, Ohgaki H, Wiestler OD, et al. The 2007 WHO classification of tumours of the central nervous system. *Acta Neuropathol.* 2007;114:97–109.
24. Cornu P, Benavides J, Scatton B, Hauw JJ, Philippon J. Increase in omega 3 (peripheral-type benzodiazepine) binding site densities in different types of human brain tumours: a quantitative autoradiography study. *Acta Neurochir (Wien).* 1992;119:146–152.
25. Herholz K, Coope D, Jackson A. Metabolic and molecular imaging in neuro-oncology. *Lancet Neurol.* 2007;6:711–724.
26. Herholz K, Langen KJ, Schiepers C, Mountz JM. Brain tumors. *Semin Nucl Med.* 2012;42:356–370.
27. Tomasi G, Edison P, Bertoldo A, et al. Novel reference region model reveals increased microglial and reduced vascular binding of ^{11}C-(*R*)-PK11195 in patients with Alzheimer's disease. *J Nucl Med.* 2008;49:1249–1256.
28. Shinozaki N, Uchino Y, Yoshikawa K, et al. Discrimination between low-grade oligodendrogliomas and diffuse astrocytoma with the aid of ^{11}C-methionine positron emission tomography. *J Neurosurg.* 2011;114:1640–1647.
29. Yamaguchi S, Kobayashi H, Hirata K, et al. Detection of histological anaplasia in gliomas with oligodendroglial components using positron emission tomography with ^{18}F-FDG and ^{11}C-methionine: report of two cases. *J Neurooncol.* 2011;101:335–341.
30. Vlodavsky E, Soustiel JF. Immunohistochemical expression of peripheral benzodiazepine receptors in human astrocytomas and its correlation with grade of malignancy, proliferation, apoptosis and survival. *J Neurooncol.* 2007;81:1–7.
31. Miettinen H, Kononen J, Haapasalo H, et al. Expression of peripheral-type benzodiazepine receptor and diazepam binding inhibitor in human astrocytomas: relationship to cell proliferation. *Cancer Res.* 1995;55:2691–2695.
32. Takaya S, Hashikawa K, Turkheimer FE, et al. The lack of expression of the peripheral benzodiazepine receptor characterises microglial response in anaplastic astrocytomas. *J Neurooncol.* 2007;85:95–103.
33. Venneti S, Lopresti BJ, Wiley CA. Molecular imaging of microglia/macrophages in the brain. *Glia.* 2013;61:10–23.
34. Wei J, Gabrusiewicz K, Heimberger A. The controversial role of microglia in malignant gliomas. *Clin Dev Immunol.* 2013;2013.
35. Kaur C, Dheen ST, Ling EA. From blood to brain: amoeboid microglial cell, a nascent macrophage and its functions in developing brain. *Acta Pharmacol Sin.* 2007;28:1087–1096.
36. Agnello D, Carvelli L, Muzio V, et al. Increased peripheral benzodiazepine binding sites and pentraxin 3 expression in the spinal cord during EAE: relation to inflammatory cytokines and modulation by dexamethasone and rolipram. *J Neuroimmunol.* 2000;109:105–111.
37. Rupprecht R, Papadopoulos V, Rammes G, et al. Translocator protein (18 kDa) (TSPO) as a therapeutic target for neurological and psychiatric disorders. *Nat Rev Drug Discov.* 2010;9:971–988.